INTERNATIONAL JOURNAL FOR NUMERICAL METHODS IN FLUIDS
Int. J. Numer. Meth. Fluids 2002; **38**:861–879 (DOI: 10.1002/fld.244)

A low-dimensional spectral approach for transient axisymmetric free-surface flow inside thin cavities of arbitrary shape

Roger E. Khayat[1,*,†] and Andreas Simanowski[2]

[1] *Department of Mechanical and Materials Engineering, The University of Western Ontario, London, Ontario, Canada N6A 5B9*
[2] *Department of Electrical and Computer Engineering, The University of Western Ontario, London, Ontario, Canada N6A 5B9*

SUMMARY

A low-dimensional spectral method is used to solve the transient axisymmetric free surface flow inside thin cavities of arbitrary shape. The flow field is obtained on the basis of the lubrication equations, which are expanded in terms of orthonormal functions over the cavity gap. The formulation accounts for nonlinearities stemming from inertia and front location. The work is of close relevance to the filling stage during die casting, and injection molding, or the flow inside annular (extrusion) dies. Both flows under an imposed flow rate, and an imposed pressure at the cavity entrance are examined. The influence of inertia, aspect ratio, gravity, and wall geometry on the evolution of the front, flow rate, and pressure is assessed particularly in the early stage of flow, when a temporal behavior of the 'boundary-layer' type develops. The multiple-scale method is applied to obtain an approximate solution at small Reynolds number, *Re*. Comparison with the exact (numerical) solution indicates a wide range of validity for the multiple-scale approach, including the moderately small *Re* range. Copyright © 2002 John Wiley & Sons, Ltd.

KEY WORDS: free surface cavity flow; die casting; injection molding

1. INTRODUCTION

The modeling and simulation of free surface cavity flow have been the object of considerable interest over the last two decades. The interest in this area of research activity is largely due to the need for new computational algorithms that assist in the design and fabrication of plastic and metal parts as encountered in the processing industry, particularly in injection molding and die casting. Modeling of the flow in these processes represents several major challenges since it is inherently transient, non-isothermal, and includes a free surface moving through cavities of highly irregular geometry. Despite the continuous development of new

*Correspondence to: R. E. Khayat, Department of Mechanical & Materials Engineering, Faculty of Engineering Science, The University of Western Ontario, London, Ontario, Canada N6A 5B9.
†E-mail: rkhayat@eng.uwo.ca

Received August 2000
Revised 19 July 2001

solution techniques, and the advent of powerful computational platforms, the simulation of free surface flow inside a cavity remains challenging. For transient free surface flow, the presence of geometrical nonlinearities, coupled to materials nonlinearities, such as inertia (die casting) and non-Newtonian (injection molding) effects, make the moving-domain problem difficult to solve and understand.

Due to limited computational resources, the three-dimensional flow problem has customarily been simplified to a two-dimensional problem, based on the observation of Hele-Shaw [1]. The method is closely related to the lubrication or shallow-water theory for Newtonian flow. In this approach, the cavity is assumed to be thin, and out of plane flows are neglected. Richardson [2] was the first to propose this method for molding flow. He examined Newtonian, isothermal flow inside cavities of simple geometry. Three decades later, the lubrication assumption remains the basis for the simulation of free surface flow of thin films [3–5]. Whilst all of the related mathematical models used in the literature stem from the common (and justifiable) assumption of constant hydrostatic pressure distribution in the vertical direction, further restrictive assumptions, which are usually introduced without quantitative justification, result in the creation of mathematical forms with different capabilities. In particular, (i) formulations in which the vertical distribution of horizontal velocity components is variable and allows the study of return flows [6], and (ii) formulations in which only the mean horizontal velocities are considered [7].

More generally, several numerical techniques have been developed for the solution of moving boundary/initial value problems. These techniques may be classified as Eulerian, Lagrangian, and mixed Eulerian–Lagrangian [8]. In the Eulerian description of the flow, the grid points remain stationary or move in a predetermined manner [9–12]. In the Lagrangian approach, the grid points move with local fluid particles [13, 14]. The free surface is sharply defined and it is easy to impose the necessary boundary conditions. However, Lagrangian methods require mesh refinement or remeshing for large deformations of the free surface. Hybrid methods have also been developed that combine the advantages of the Eulerian and Lagrangian methods [15]. Generally, an adaptive Lagrangian approach becomes difficult to implement when a volume method such as the finite-element method (FEM) is used. On the other hand, the boundary-element method (BEM) is much easier to use along with adaptive remeshing as the dimension of the problem is reduced by one. The advantages of the BEM include: reduction of problem dimensionality, direct calculation of the interfacial velocity, the ability to track large surface deformations, and the potential for easy incorporation of interfacial tension as well as other surface effects [16–18]. However, there are a number of simplifying assumptions that are customarily adopted for the BEM to become applicable. Nonlinear effects are difficult to account for in a boundary-element approach despite the advent of recent techniques to handle nonlinear and transient problems [19–22].

Regarding the simulation of free surface flows with inertia, one is faced, on the one hand, with the incapacity of conventional domain methods to deal with the issue of adaptive meshing for moving-boundary flows and, on the other hand, with the failure of the BEM to deal with nonlinearities stemming from inertia and upper-convected terms. The present paper addresses the solution of a large class of axisymmetric free-surface flows with close relevance to materials processing, in particular die casting and injection molding. The flow problems are typically concerned with the filling stage inside a thin cavity. The lubrication assumption is adopted to derive the relevant conservation equations, which are averaged over the cavity gap. The flow in the gap direction is not neglected. This study focuses on the early transients

in free surface thin-cavity flow. The rapid evolution of pressure and flow rate in the initial flow stage are examined in detail.

2. PROBLEM FORMULATION, GENERAL EQUATIONS, BOUNDARY AND INITIAL CONDITIONS

In this section, the lubrication equations, as well as the boundary and initial conditions, are briefly reviewed for transient axisymmetric free surface flow inside a cavity of arbitrary shape as depicted in Figure 1.

2.1. Governing equations

Consider an incompressible Newtonian viscous fluid of density ρ, and viscosity μ. Surface tension effect is assumed to be negligible. A section of the flow is schematically illustrated in Figure 1, where (R, Θ, X) denote the cylindrical coordinates. The inner and outer cylindrical rigid surfaces of the cavity are given by $R_1(X)$ and $R_2(X)$, respectively. The flow may be induced by the action of an imposed flow rate, a driving pressure at the cavity entrance, and/or gravity. The emphasis in this study, however, will be on the flow induced by an imposed flow rate. The continuity equation reads:

$$U_{R,R} + \frac{1}{R}U_R + U_{X,X} = 0 \tag{1}$$

where U_R and U_X are the radial and axial components of velocity. The relevant equations from the conservation of momentum are

$$\rho(U_{R,T} + U_R U_{R,R} + U_X U_{R,X}) = -\Pi_{,R} + \mu\left(U_{R,RR} + \frac{U_{R,R}}{R} - \frac{U_R}{R^2} + U_{R,XX}\right) \tag{2a}$$

$$\rho(U_{X,T} + U_R U_{X,R} + U_X U_{X,X}) = -\Pi_{,X} + \mu\left(U_{X,RR} + \frac{U_{X,R}}{R} + U_{X,XX}\right) + \rho g \tag{2b}$$

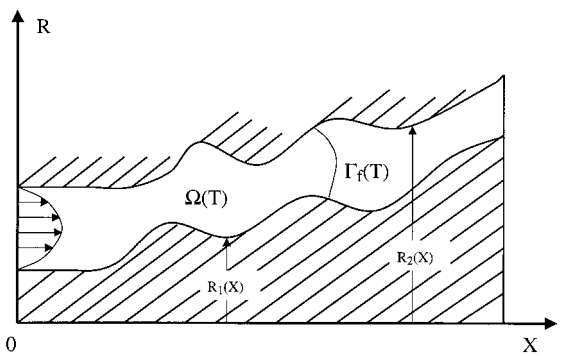

Figure 1. Schematic view and notations used for typical moving-boundary flow and confining axisymmetric thin cavity.

where a subscript after the comma denotes partial differentiation. T is the time, Π is the dynamic pressure, and g is the acceleration due to gravity, which is assumed to act in the positive X direction.

The conservation equations above are now formulated in the narrow-gap limit. The dimensionless variables are introduced as follows:

$$\begin{aligned} x &= \frac{X}{R_0}, \qquad z = \frac{R - R_0}{D_0}, \qquad t = \frac{V}{R_0} T \\ u_x &= \frac{U_x}{V}, \qquad u_z = \frac{U_R}{V\varepsilon}, \qquad p = \frac{\varepsilon^2 R_0}{\mu V} \Pi \end{aligned} \tag{3}$$

where $R_0 = R_1(X = 0)$ is the radius of the inner cylinder at the entrance, $D_0 = R_2(X = 0) - R_1(X = 0)$ is the gap at the entrance, $\varepsilon = D_0/R_0$ is the (typical) aspect ratio, and V is a typical reference velocity, which is related to the applied flow rate or the pressure at the entrance to the cavity, depending on the case studied. In addition to ε, there are two important dimensionless groups, namely, the Reynolds number, Re, and the Froude number, Fr. The parameters for the problem are explicitly written here:

$$Re = \frac{\rho V R_0}{\mu} \varepsilon^2, \quad \varepsilon = \frac{D_0}{R_0}, \quad Fr = \frac{V}{\sqrt{g R_0}} \tag{4}$$

In lubrication theory, Re is sometime referred to as the modified Reynolds number [23]. In dimensionless form, and if terms of $O(\varepsilon^2)$ and higher are excluded, then Equations (1) and (2) reduce to:

$$u_{x,x} + \varepsilon u_z + u_{z,z} = 0 \tag{5}$$

$$Re(u_{x,t} + u_x u_{x,x} + u_z u_{x,z}) = Re/Fr^2 - p_{,x} + u_{x,zz} + \varepsilon u_{x,z} \tag{6a}$$

$$p_{,z} = 0 \tag{6b}$$

The term Re is not necessarily negligible, even for small ε, since inertia effects may be large enough for the modified Reynolds number to be of order one. In this study, most numerical results are reported for $Re = O(1)$.

2.2. Boundary and initial conditions

Let the front be represented by $x = F(z,t)$. The domain of computation is given by $\Omega(t) = \{(x,z) \,|\, x \in [0, F(z,t)],\ z \in [z_1(x), z_2(x)]\}$, where $z_1(x) = [R_1(x) - R_0]/D_0$ and $z_2(x) = [R_2(x) - R_0]/D_0$. Note that if terms of $O(\varepsilon)$ are neglected, the formulation reduces to that corresponding to two-dimensional flow [23].

The boundary conditions for system (5)–(6) include the no-slip conditions at the inner and outer cylinders, the exit conditions at $x = 0$, and the dynamic and kinematic conditions at the front. Thus, at the rigid surfaces:

$$u_x(x, z = z_1, t) = u_x(x, z = z_2, t) = u_z(x, z = z_1, t) = u_z(x, z = z_2, t) = 0 \tag{7}$$

It is assumed that the flow at the channel exit, at $x=0$, satisfies Poiseuille flow, that is the flow inside an infinite annular die, leading to the following expressions:

$$u_x(x=0,z,t)=\frac{6(2-\varepsilon)Q(t)}{2+\varepsilon}z\left(1-\frac{\varepsilon}{3}-z+\frac{\varepsilon}{3}z^2\right),\quad u_z(x=0,z,t)=0 \tag{8}$$

where $Q(t)$ is the imposed flow rate. In the absence of surface tension, the traction must vanish at the free surface. To leading order in ε, the dynamic condition reduces to the vanishing of the pressure:

$$p(x=F,z,t)=0 \tag{9}$$

The kinematic condition used in this study is given by

$$u_x(x=F,z,t)=\frac{\mathrm{d}F(z,t)}{\mathrm{d}t} \tag{10}$$

As to the initial conditions, the fluid is assumed to be in general initially at rest (stress free), occupying a finite domain. However, there are situations when acceleration (inertia) vanishes if the applied flow rate is constant. In this case, the initial flow at $t=0$ must immediately adjust to the applied driving force.

3. SOLUTION PROCEDURE

The solution of the problem is obtained by expanding the flow field over the cavity thickness. The resulting equations for the expansion coefficients are integrated between the cavity entrance and front location along the axial direction. The problem then reduces to a nonlinear coupled system that governs the evolution of the front location, $L(t)$, flow rate, $Q(t)$, and entrance pressure, $P(t)$.

3.1. Elimination of the z dependence

System (5)–(10) is now reduced to a transient one-dimensional problem by expanding the flow variables in terms of appropriately chosen orthonormal modes in the z direction, and applying the Galerkin projection method to generate the equations that govern the expansion coefficients. The procedure is closely related to that suggested by Zienkiewicz and Heinrich in shallow-water theory [4]. In particular, it is assumed that the flow in the axial direction, x, can be represented by a contribution of some suitably selected orthonormal shape functions, such that:

$$u_x(x,z,t)=\sum_{i=1}^{M}U_i(x,t)\phi_i(\xi) \tag{11}$$

where M is the number of modes, $\xi=(2z-\Sigma(x))/2\Delta(x)$ is the normalized transverse coordinate, $U_{i\in[1,M]}$ are the expansion coefficients, and $\phi_{i\in[1,M]}$ are the shape functions. Here $\Delta(x)=z_2(x)-z_1(x)$ and $\Sigma(x)=z_2(x)+z_1(x)$. In this case, $\xi\in[-1/2,+1/2]$. The radial component of the velocity, u_z, is determined by inserting expression (11) into Equation (5) and

integrating over the interval $[-1/2, \xi]$, such that

$$u_z(x,z,t) = -\Delta\sum_{i=1}^{M}[(1-\varepsilon\Delta\xi)F_i + \varepsilon\Delta G_i]U_{i,x} + \sum_{i=1}^{M}\left\{\frac{\Sigma_{,x}}{2}(1-\varepsilon\Delta\xi)\phi_i + \varepsilon\Delta\Delta_{,x}(\xi^2\phi_i - 2G_i) + \left[\Delta_{,x} + \varepsilon\Delta\left(\frac{\Sigma_{,x}}{2} - \Delta_{,x}\xi\right)\right](\xi\phi_i - F_i)\right\}U_i \tag{12}$$

where $F_i(\xi) = \int_{-1/2}^{\xi}\phi_i\,\mathrm{d}\xi$, and $G_i(\xi) = \int_{-1/2}^{\xi}\xi\phi_i\,\mathrm{d}\xi$.

The equations that govern the expansion coefficients, $U_i(x,t)$, are derived by using the Galerkin projection method, which consists of inserting expressions (11) and (12) into Equation (6a), multiplying the equation by $\phi_i(\xi)$, and integrating over the interval $\xi \in [-1/2, +1/2]$, to give

$$U_{i,t} + \sum_{j=1}^{M}\sum_{k=1}^{M}\left\{[\langle\phi_i(\phi_j\phi_k - F_j\phi_k')\rangle + \varepsilon\Delta\langle\phi_i(G_j - \xi F_j)\phi_k'\rangle]U_jU_{k,x} + \left[\left(\frac{\Delta_{,x}}{\Delta} + \varepsilon\frac{\Sigma_{,x}}{2}\right)\langle\phi_iF_j\phi_k'\rangle - \varepsilon\Delta_{,x}\langle\phi_i(\xi F_j - 2G_j)\phi_k'\rangle\right]U_jU_k\right\} = \left(\frac{1}{Fr^2} - \frac{1}{Re}p_{,x}\right)\langle\phi_i\rangle + \frac{1}{\Delta Re}\sum_{j=1}^{M}\left[\varepsilon\langle\phi_i\phi_j'\rangle + \frac{1}{\Delta}\langle\phi_i\phi_j''\rangle\right]U_j \tag{13}$$

where $\langle\,\rangle = \int_{-1/2}^{1/2}\mathrm{d}\xi$.

3.2. Elimination of the x dependence

The x dependence of the coefficients $U_i(x,t)$ is determined explicitly by integrating Equation (5) in the z direction and applying the no-slip condition at $z_1(x)$ and $z_2(x)$. In particular, one obtains the following equation that relates the coefficients at an arbitrary axial location to the coefficients at the mean front position, $L(t)$, which states that the flow rate, $Q(t)$, is conserved at any location:

$$Q(t) = \sum_{i=1}^{M}\chi_i(x)U_i(x,t) = \sum_{i=1}^{M}\chi_i(L)U_i^L(t) \tag{14}$$

where $U_i^L(t) = U_i(x=L,t)$, and $\chi_i(x) = \Delta(x)(1+\frac{\varepsilon}{2}\Sigma(x))\langle\phi_i\rangle + \varepsilon\Delta^2(x)\langle\xi\phi_i\rangle$. A solution of Equation (14) that satisfies the problem for an arbitrary number of modes is given by

$$U_i(x,t) = \frac{\chi_i(L)}{\chi_i(x)}U_i^L(t), \quad i \in [1,M] \tag{15}$$

The x dependence of the radial velocity component ensues by substituting expression (15) into (12). Note, however, that unlike $u_x(x,z,t), u_z(x,z,t)$ is not separable in x and t.

Given the explicit dependence of $U_i(x,t)$ on x, the equations that govern the time-dependent coefficients $U_i^L(t)$ are obtained by substituting expression (15) into Equation (13), integrating

the latter over the interval $x \in [0, L]$, and using condition (9), thus leading to the following system of ordinary differential equations:

$$A_i \frac{\mathrm{d}U_i^L}{\mathrm{d}t} + B_i U_i^L + \sum_{j=1}^{M}\sum_{k=1}^{M} C_{ijk} U_j^L U_k^L = \left(\frac{L}{Fr^2} - \frac{P}{Re}\right)\langle\phi_i\rangle + \frac{1}{Re}\sum_{j=1}^{M} D_{ij} U_j^L \tag{16}$$

where $P(t) = p(x = 0, t)$ is the pressure at the channel exit. The time dependent matrix coefficients are given by:

$$A_i(t) = \chi_i(L)\int_0^L \frac{\mathrm{d}x}{\chi_i}, \quad B_i(t) = -\frac{\chi_i(L)}{\Delta(L)}\left(\sum_{j=1}^{M}\chi_j(L)U_j^L(t)\right)\int_0^L \frac{\chi_i'\,\mathrm{d}x}{\chi_i^2}$$

$$\begin{aligned} C_{ijk}(t) = {} & \chi_j(L)\chi_k'(L)\left[\langle\phi_i(\phi_j\phi_k - F_j\phi_k')\rangle\int_0^L \frac{\chi_k'}{\chi_j\chi_k^2}\,\mathrm{d}x + \varepsilon\langle\phi_i(G_j - \xi F_j)\phi_k'\rangle\int_0^L \frac{\Delta\chi_k'}{\chi_j\chi_k^2}\,\mathrm{d}x\right] \\ & + \chi_j(L)\chi_k(L)\left[\langle\phi_i F_j\phi_k'\rangle\int_0^L \left(\frac{\Delta_{,x}}{\Delta} + \varepsilon\frac{\Sigma_{,x}}{2}\right)\frac{\mathrm{d}x}{\chi_j\chi_k} - \varepsilon\langle\phi_i(\xi F_j - 2G_j)\phi_k'\rangle\int_0^L \frac{\Delta_{,x}}{\chi_j\chi_k}\,\mathrm{d}x\right] \\ D_{ij}(t) = {} & \chi_j(L)\left(\varepsilon\langle\phi_i\phi_j'\rangle\int_0^L \frac{\mathrm{d}x}{\Delta\chi_j} + \langle\phi_i\phi_j''\rangle\int_0^L \frac{\mathrm{d}x}{\Delta^2\chi_j}\right) \end{aligned} \tag{17}$$

The expression of the mean front position, $L(t)$, is obtained by averaging kinematic condition (10) over the cross section, leading to:

$$\frac{\mathrm{d}L}{\mathrm{d}t} = \frac{1}{\Delta(L)}\int_{z_1(L)}^{z_2(L)} (1 + \varepsilon z)u_x(x = L, z, t)\,\mathrm{d}z \tag{18}$$

which is obviously related to the flow rate:

$$\frac{\mathrm{d}L}{\mathrm{d}t} = \frac{Q(t)}{\Delta(L)} \tag{18a}$$

and, consequently from Equation (14), to the velocity coefficients:

$$\frac{\mathrm{d}L}{\mathrm{d}t} = \frac{1}{\Delta(L)}\sum_{i=1}^{M}\chi_i(L)U_i^L(t) \tag{18b}$$

The differential-algebraic system (14), (16) and (18) involves $M + 2$ equations, governing $M + 3$ unknowns, namely, $U_1^L, \ldots, U_M^L$, Q, P and L. Obviously, one of these quantities will have to be prescribed. There are two categories of problems envisaged generally in cavity flow: (i) the flow that is induced at a prescribed flow rate, $Q(t)$, and (ii) the flow that is due to an imposed pressure, $P(t)$, at the cavity entrance, $x = 0$. In both cases, the initial conditions are only imposed on the velocity and front position. In general,

$$U_i^L(t = 0) = U_i^{L_0}, \quad L(t = 0) = L_0 \tag{19}$$

where L_0 is the mean front position of the initial fluid domain.

If P is prescribed, then Equations (16) and (18b) are solved subject to initial conditions (19), and the flow rate is then evaluated from expression (14). Although in this case the problem reduces to the solution to a set of ordinary differential equations that is not difficult

to obtain, the prescription of pressure at the entrance is not generally the route adopted in practice. In this study, the flow rate will be assumed to be prescribed with time. The unknowns in the problem are then the velocity coefficients, the pressure at the entrance, and the mean front position. This is the more difficult problem since it involves the simultaneous solution of a differential-algebraic system. However, the problem is reduced to a differential system of equations by differentiating Equation (14) with respect to t, and substituting for $\mathrm{d}U_i^L/\mathrm{d}t$ and $\mathrm{d}L/\mathrm{d}t$ from Equations (16) and (18a), respectively, to obtain an expression for P in terms of U_i^L and L alone. This expression, in turn, is then substituted in Equations (16) to eliminate P, leading to the system of differential equations for U_i^L and L. The derivation is algebraically involved and not illuminating. Only details with relevance to the special case of a straight annular cavity will be given (see below). The resulting system is solved as an initial-value problem subject to conditions (19), using a sixth-order Runge–Kutta integration scheme (IMSL-DIVPRK). The integrals in expressions (17) were evaluated using a globally adaptive integration scheme based on Gauss–Kronrod rules (IMSL-DQDAG). The tolerance used for both schemes is 10^{-5}. Note that in this case, L is decoupled from the velocity coefficients, and is obtained upon solving Equation (18a) separately.

3.3. *Orthonormal functions*

The choice of appropriate orthonormal functions constitutes a crucial step in any spectral representation of the solution. These functions are usually chosen to be smooth, preferably infinitely differentiable, such as trigonometric or hyperbolic functions. In this study, the formulation follows closely that of Zienkiewicz and Heinrich [4], which includes the depth-averaging approach usually adopted in the literature on film flow. In two-dimensional flow, the axial velocity component, u_x, is assumed to be parabolic with respect to z; this assumption is based on the solution to plane Poiseuille flow. A similar approach may be adopted for the present problem, where a parabolic and a cubic shape function may be assumed for the two leading modes, in reference to the Poiseuille flow in an annular die. In general the modes are taken to satisfy:

$$\phi_i\left(\xi = \pm\frac{1}{2}\right) = 0, \qquad \langle\phi_i\phi_j\rangle = \delta_{ij}, \quad \forall i,j \in [1,M] \tag{20}$$

where δ_{ij} is the Kronecker delta. The leading mode is then taken as

$$\phi_1(\xi) = \sqrt{30}\left(\xi^2 - \frac{1}{4}\right) \tag{21}$$

The second leading mode, $\phi_2(\xi)$, may be taken cubic or a general odd function in ξ, and must be orthogonal to all other modes. There is a wide range of possibilities for the choice of the higher order orthogonal modes. These modes, however, must be odd in order to ensure their orthogonality to $\phi_1(\xi)$. In this study, odd Chandrasekhar functions will be used [24] for $\phi_{i>1}$. These functions ensure the satisfaction of the no-slip boundary conditions at $z = z_1(x)$ and $z = z_2(x)$, and have been widely used in linear and nonlinear problems, for their effectiveness in solution representation and relative high rate of convergence. Thus,

$$\phi_{i>1}(\xi) = \frac{\sinh(a_i\xi)}{\sinh(a_i/2)} - \frac{\sin(a_i\xi)}{\sin(a_i/2)} \tag{22}$$

where the constants a_i are the roots of $\coth(a_i/2) - \cot(a_i/2) = 0$.

It is argued that any arbitrary number of modes can be introduced, each satisfying the no-slip conditions at the two rigid cylindrical surfaces, but reasonable radial distributions can be obtained with $M=2$ or 3 for most practical applications [4]. Of course, the rate of convergence will strongly depend on the choice of the modes. In addition, given the small thickness of the fluid film, the flow field is not expected to vary strongly with the height z; a minimal number of modes is thus sufficient.

3.4. The special case of an annular cavity with straight walls

Considerable simplification results for a flow inside an annular die with straight walls. However, extensive results will also be given in the next section for a cavity with variable wall shape. For a boundary with straight walls, $z_1(x)=0$ and $z_2(x)=1$, so that $\Delta=\Sigma=1$. In this case, $\chi_i(x)=\chi_i(L)=(1+\varepsilon/2)\langle\phi_i\rangle+\varepsilon\langle\xi\phi_i\rangle$. It is not difficult to show, upon substituting expressions (11) and (12) into Equation (5), that $u_z(x,z,t)=0$. The vanishing of u_z leads in turn, again from Equation (5), to $u_{x,x}(x,z,t)=0$. Thus, u_x is independent of x, and therefore $U_i(x,t)=U_i^L(t)$. The nonlinear convective terms also vanish, and Equation (16) reduces to

$$\frac{\mathrm{d}U_i^L}{\mathrm{d}t}=\left(\frac{1}{Fr^2}-\frac{P}{Re\,L}\right)\langle\phi_i\rangle+\frac{1}{Re}\sum_{j=1}^{M}(\varepsilon\langle\phi_i\phi_j'\rangle+\langle\phi_i\phi_j''\rangle)U_j^L \tag{23}$$

In this case, P is given by

$$P(t)=\frac{Re\,L}{Fr^2}-\frac{L}{\langle\phi_1\rangle\chi_1}\left[Re\frac{\mathrm{d}Q}{\mathrm{d}t}-\sum_{i=1}^{M}\sum_{j=1}^{M}\chi_i(\varepsilon\langle\phi_i\phi_j'\rangle+\langle\phi_i\phi_j''\rangle)U_j^L\right] \tag{24}$$

which, upon substitution into Equation (23), and in combination with Equation (18), leads to the desired dynamical system.

$$\frac{\mathrm{d}U_i^L}{\mathrm{d}t}=\frac{\langle\phi_i\rangle}{\langle\phi_1\rangle\chi_1}\frac{\mathrm{d}Q}{\mathrm{d}t}+\frac{1}{Re}\sum_{j=1}^{M}\sum_{k=1}^{M}\left(\delta_{ik}-\frac{\langle\phi_i\rangle\chi_k}{\langle\phi_1\rangle\chi_1}\right)(\varepsilon\langle\phi_k\phi_j'\rangle+\langle\phi_k\phi_j''\rangle)U_j^L \tag{25}$$

In this case, the front position is dictated by Equation (18a), which reduces to

$$\frac{\mathrm{d}L}{\mathrm{d}t}=Q(t) \tag{26}$$

which is integrated once $Q(t)$ is specified.

4. NUMERICAL ASSESSMENT AND RESULTS

The general formulation above is now implemented for the problem of transient flow of a fluid penetrating a thin cavity as depicted in Figure 1. Both the flow in an annular straight channel, and a cavity with variable thickness will be considered. The flow with small inertia will be examined in some detail when a pressure is imposed for a cavity with straight walls. The effect of wall geometry on the flow inside a contracting, and an expanding walled cavity will be examined. In all results reported, the initial domain is assumed to be straight with $L(t=0)=0$. The flow rate is imposed, so that $Q(t)=1$.

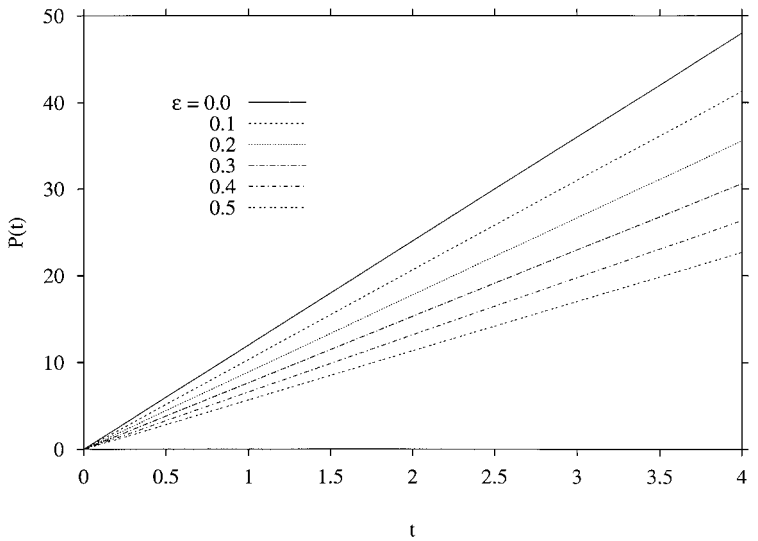

Figure 2. Influence of the aspect ratio on the evolution of the pressure, $P(t)$, at the channel exit, for a flow inside a straight-walled cavity, for the range $\varepsilon \in [0, 0.5]$, and $M = 4$.

4.1. *Flow inside a straight-walled annular channel*

Consider the flow induced by a constant flow rate inside a cavity with straight walls. In this case, the front moves at a constant speed, and the pressure at the channel exit, $P(t)$, is the main unknown in the problem. The flow rate is taken (normalized) $Q(t) = 1$. In this case, the only quantity that depends on time is L, which is given from Equation (18):

$$L(t) = t + L_0 \tag{27}$$

It is clear from Equation (25) that, when the flow rate is constant, the fluid cannot be assumed to be at rest initially. Indeed, if $U_i^{L_0} = 0$ for any $i \in [1, M]$, then the initial and subsequent acceleration terms remain zero since the system of equations is homogeneous. In this case, non-homogenous conditions must be given, which correspond to the immediate adjustment of the flow to the imposed flow rate at $t > 0$. Thus,

$$U_i^{L_0} = \frac{6(2-\varepsilon)}{2+\varepsilon} \left\langle z \left(1 - \frac{\varepsilon}{3} - z + \frac{\varepsilon}{3} z^2\right) \phi_i \right\rangle \tag{28}$$

where the first of expressions (8) is used. The influence of ε is depicted from Figure 2, where the evolution of the pressure is shown for $\varepsilon \in [0, 0.5]$ and $Re = 1$, over a period of four time units. The figure shows that the front evolves at a slower rate as the aspect ratio increases. The two-dimensional behavior is recovered by the curve corresponding to $\varepsilon = 0$, where the pressure increases at a rate equal to 12. It is interesting to observe from Figure 2 that although the rate $\mathrm{d}P/\mathrm{d}t$ decreases monotonically as ε increases, this decrease varies asymptotically.

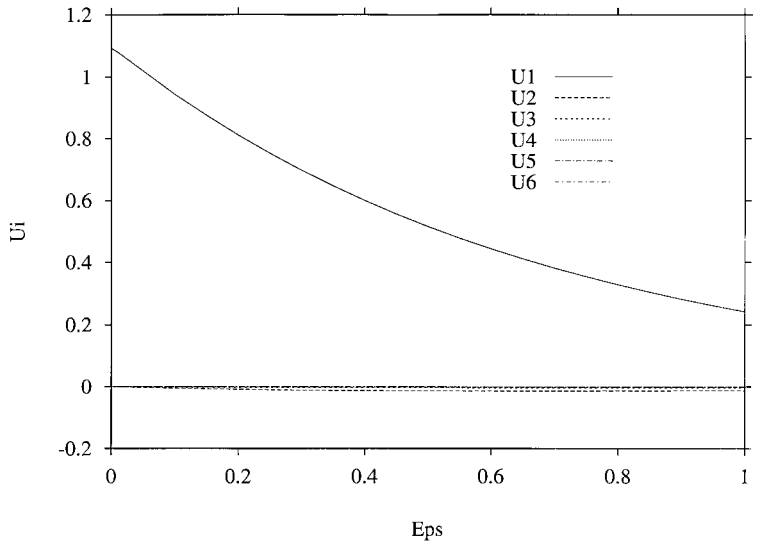

Figure 3. Evolution of the velocity coefficients for a flow inside a straight-walled cavity, $Re = 1$ and $\varepsilon = 0.5$. Here $M = 6$.

The convergence of the method is assessed by monitoring the magnitude of the leading and higher order modes. Figure 3 displays the value of the velocity coefficients for $M = 6$, as functions of the aspect ratio. Note that the velocity coefficients remain essentially constant with time, at least over the period considered. It is clear from the figure that six modes are entirely sufficient for the whole range of ε, since only U_1^L and (to a much lesser extent) U_2^L are essentially the non-zero modes. Note, however, the discrepancy between the leading and higher order modes decreases significantly as ε increases. It will be seen below that convergence depends on the aspect ratio and inertia but is generally achieved for $M < 4$.

4.2. *Influence of wall geometry*

In this section, the effect of wall geometry will be examined for expanding and contracting cavities. The inner cylinder is assumed to remain straight (parallel to the x axis). Thus, $z_1(x) = 0$, and $z_2(x) = 1 + axH(x)$, where $a > 0$ is the constant slope of the outer wall, and H is the Heavyside function.

Consider first the flow inside a contracting cavity ($a < 0$). The evolution of the pressure at the channel exit, $P(t)$, is typically illustrated in Figure 4 for $Re = 10$, $\varepsilon = 0.5$, and $a = -1/50$. Five different truncation levels are used to assess the convergence of the results in this case, corresponding to $M \in [2, 10]$. The figure shows the typical exponential-like growth over 20 time units. The inset in the figure shows the curves in the range $t \in [16.9, 17]$, which clearly indicates that convergence is essentially achieved for $M > 2$. The pressure tends to be generally underestimated. Figure 5 shows the relative dominance of the two leading-order modes, U_1^L and (to a much lesser extent) U_2^L when six modes are included, particularly at the stage of flow. Observe the very slight dependence on time of $U_{i>1}^L$, despite the significant deviation of $P(t)$ from linear growth.

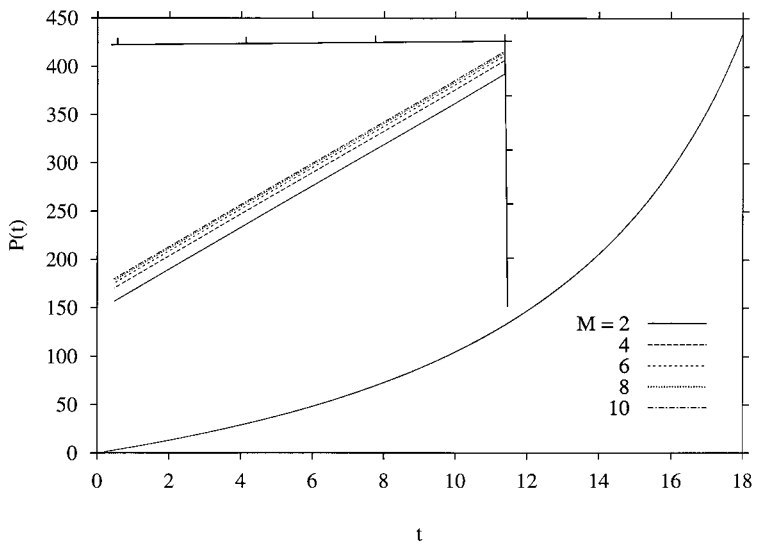

Figure 4. Convergence assessment for a flow inside a contracting cavity of slope $a=-1/50$, $Re=10$ and $\varepsilon=0.5$. The figure displays the evolution of $P(t)$ for $M\in[2,10]$. Inset shows the range $t\in[16.94,17]$.

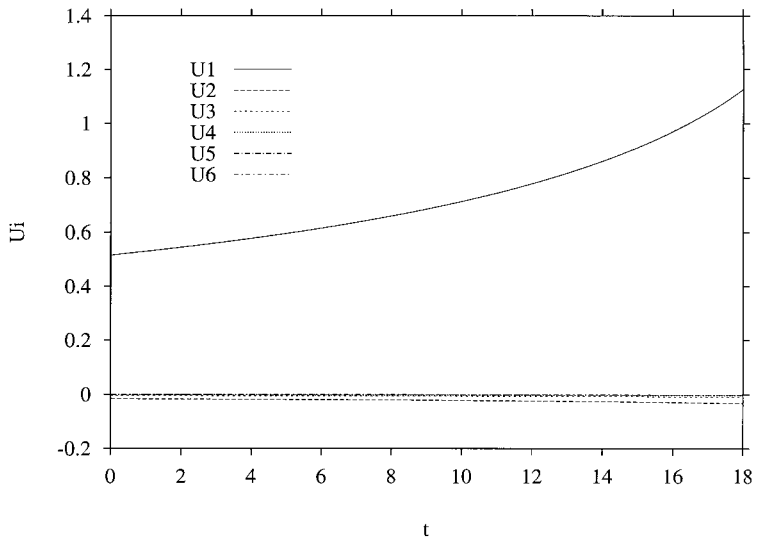

Figure 5. Evolution of the velocity coefficients for a flow inside a contracting cavity of slope $a=-1/50$, $Re=10$, $\varepsilon=0.5$ and $M=6$.

The influence of inertia on the contracting flow is illustrated in Figure 6. The figure shows $P(t)$ for the flow inside a cavity with $\varepsilon=0.5$ and $a=-1/50$, for the range $Re\in[1,100]$. The results are based on $M=6$. As expected, the growth rate in pressure increases for a flow with higher inertia. The growth rate is found to increase essentially linearly with Re. The influence

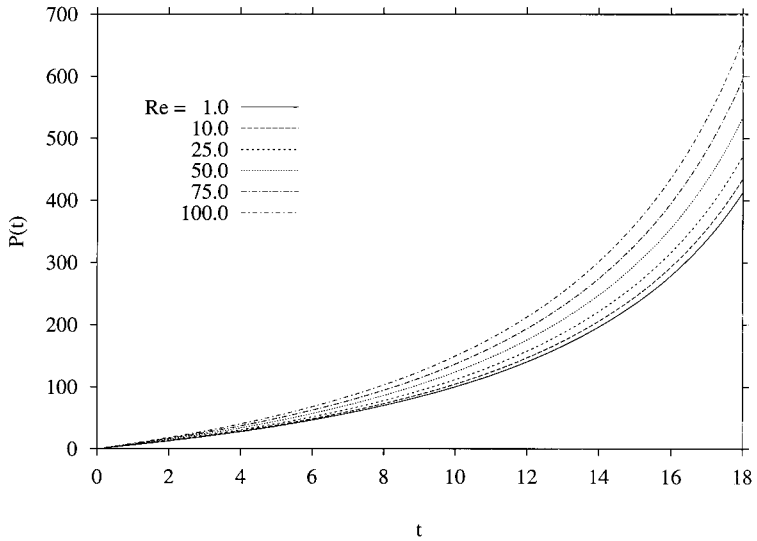

Figure 6. Influence of inertia on the evolution of the pressure, $P(t)$, at the channel exit, for a flow inside a contracting cavity, for the range $Re \in [1, 100]$, $\varepsilon = 0.5$, $a = -1/50$ and $M = 6$.

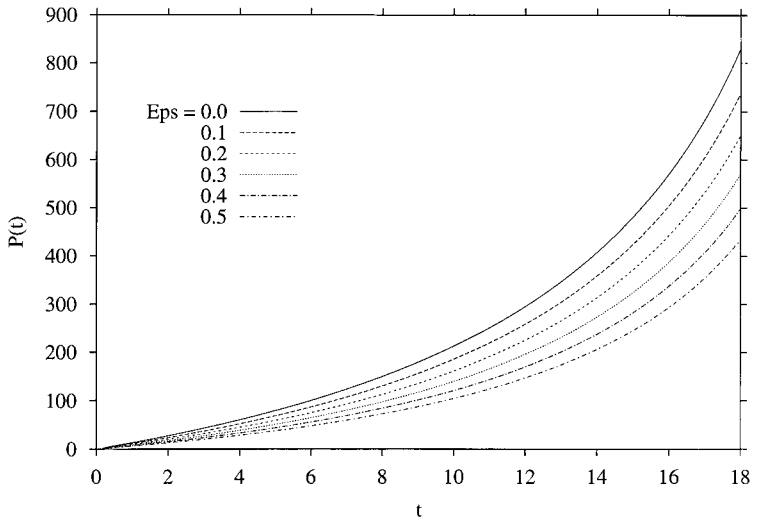

Figure 7. Influence of the aspect ratio on the evolution of the pressure, $P(t)$, at the channel exit, for a flow inside a contracting cavity, for the range $\varepsilon \in [0.1, 0.5]$, $Re = 10$, $a = -1/50$ and $M = 6$.

of aspect ratio is depicted from Figure 7, for $Re = 10$, $a = -1/50$, $M = 6$, and $\varepsilon \in [0, 0.5]$. Recall that $\varepsilon = 0$ corresponds to two-dimensional flow. The pressure tends to build up more strongly for the smaller gap cavity. Unlike the dependence on inertia, the rate of pressure increase diminishes as the aspect ratio increases.

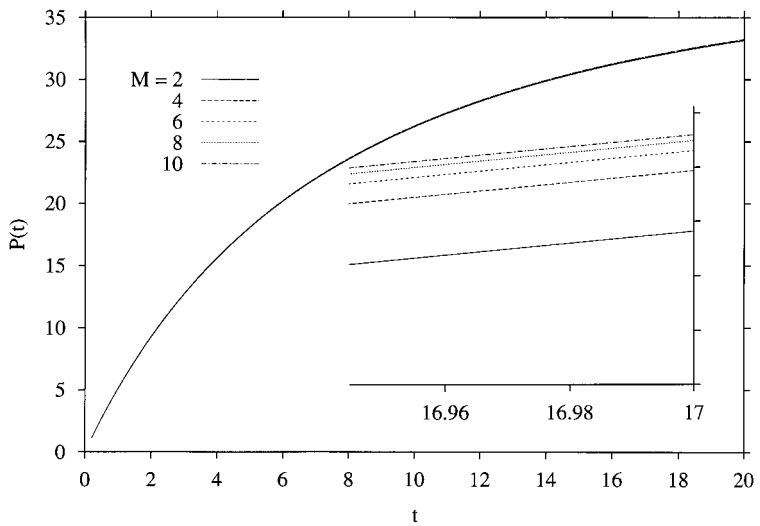

Figure 8. Convergence assessment for a flow inside an expanding cavity of slope $a = 1/20$, $Re = 0.1$ and $\varepsilon = 0.5$. The figure displays the evolution of $P(t)$ for $M \in [2, 10]$. Inset shows the range $t \in [16.94, 17]$.

Consider now the flow inside an expanding cavity ($a > 0$). The evolution of the pressure at the channel exit, $P(t)$, is typically illustrated in Figure 8 for $Re = 0.1$, $\varepsilon = 0.5$, and $a = 1/20$. Five different truncation levels are used to assess the convergence of the results in this case, corresponding to $M \in [2, 10]$. The figure shows the typical logarithmic-like growth over 20 time units, which should be contrasted with Figure 4. The inset in the figure shows the curves in the range $t \in [16.9, 17]$, indicating that convergence is essentially again achieved for $M > 2$. The pressure is generally again underestimated. Figure 9 shows the relative dominance of the two leading-order modes, U_1^L and U_2^L when six modes are included. However, in contrast to Figure 5, the higher order modes, particularly $M < 5$ remain relatively influential. In addition, the time dependence of the velocity coefficients is strong. Figure 9 indicates that while U_1^L decreases with time, the remaining modes tend to increase strongly initially, but eventually reach the steady state.

The influence of inertia on the expanded flow is illustrated in Figure 10. The figure shows $P(t)$ for the flow inside a cavity with $\varepsilon = 0.1$ and $a = 1/25$, for the range $Re \in [1, 100]$. The results are based on $M = 6$. In this case (compare with Figure 6), the growth rate in pressure decreases for a flow with higher inertia. The growth rate is found to decrease essentially linearly with Re. At a critical Reynolds number, $Re \approx 100$, the pressure increases linearly with time. The influence of aspect ratio is depicted from Figure 11, for $Re = 100$, $a = 1/25$, $M = 6$, and $\varepsilon \in [0, 0.5]$. The pressure tends to drop significantly as ε decreases.

Finally, the overall influence of the slope is depicted from Figure 12. The figure displays the evolution of the pressure for a flow with $Re = 10$ and $\varepsilon = 0.5$. The results are based on $M = 6$. Negative as well as positive slopes of the outer cylinder are considered, including the case of a straight cylinder (slope $= 0$), which gives a rate of increase equal to 12. The most remarkable observation in the figure is the difference in influence of the slope between

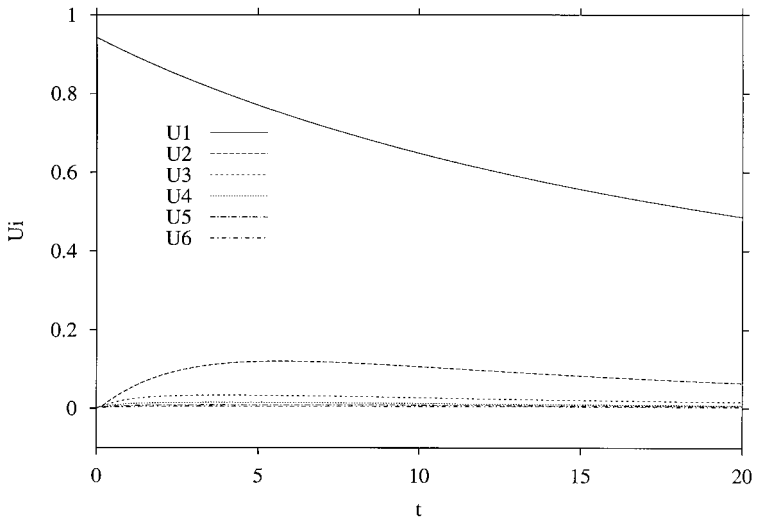

Figure 9. Evolution of the velocity coefficients for a flow inside an expanding cavity of slope $a = 1/25$, $Re = 100$, $\varepsilon = 0.5$ and $M = 6$.

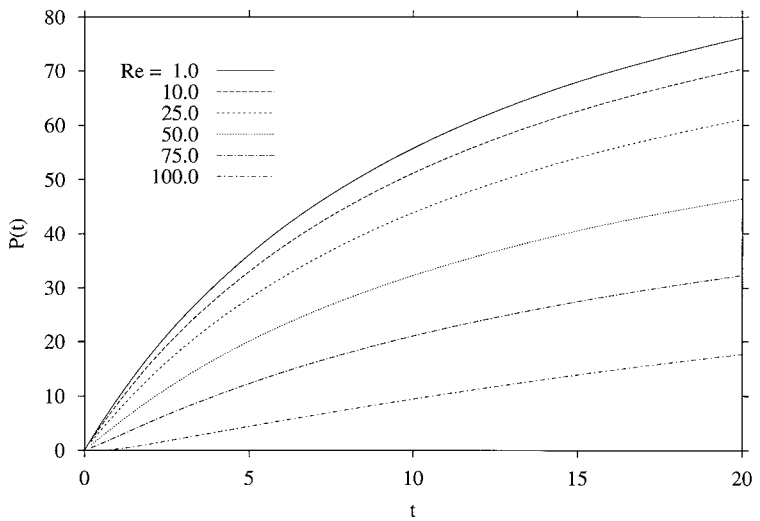

Figure 10. Influence of inertia on the evolution of the pressure, $P(t)$, at the channel exit, for a flow inside an expanding cavity, for the range $Re \in [1, 100]$, $\varepsilon = 0.1$, $a = 1/25$ and $M = 6$.

a contracting flow and an expanding flow. In the former case, a decrease in slope (from zero) leads to a rapid increase in the evolution rate of the pressure; whereas for an expanding flow, the influence of the slope is relatively insignificant.

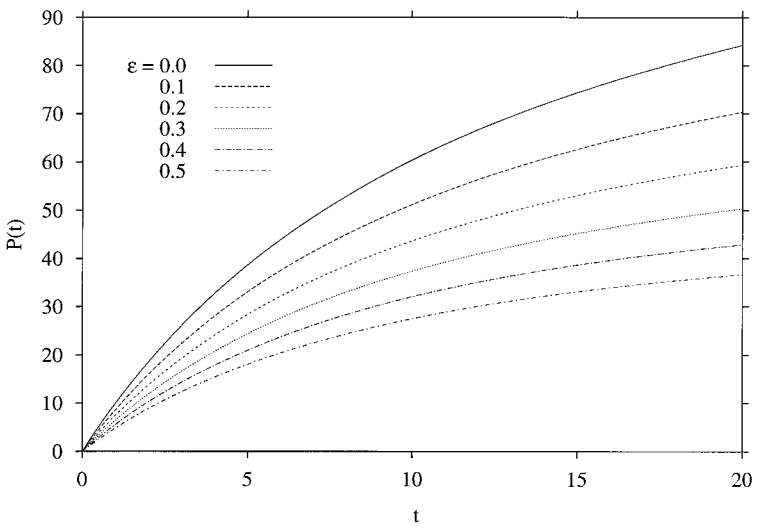

Figure 11. Influence of the aspect ratio on the evolution of the pressure, $P(t)$, at the channel exit, for a flow inside an expanding cavity, for the range $\varepsilon \in [0, 0.5]$, $Re = 100$, $a = -1/25$ and $M = 6$.

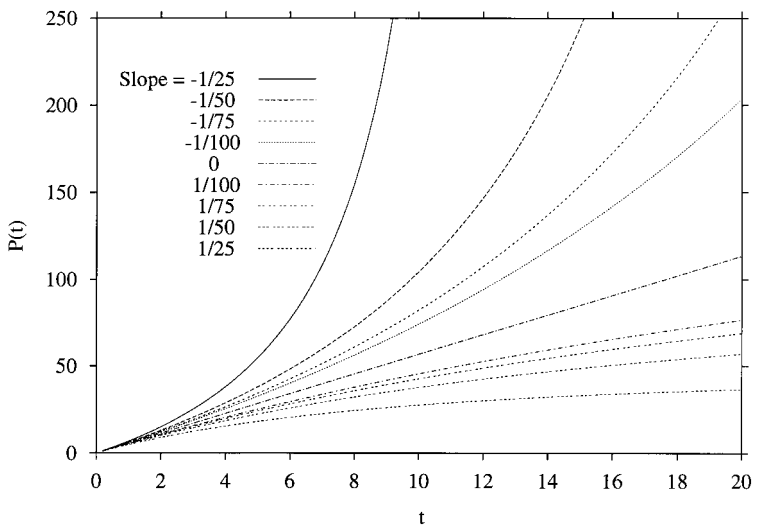

Figure 12. Influence of the outer cylinder slope on the pressure, $P(t)$, at the channel exit, for the range $a \in [-1/25, 1/25]$ of the slope, $\varepsilon = 0.5$, $Re = 10$ and $M = 6$.

5. DISCUSSION AND CONCLUSION

The influence of inertia, aspect ratio, and cavity geometry are examined on the transient axisymmetric free surface flow inside a thin cavity. The general lubrication equations for de-

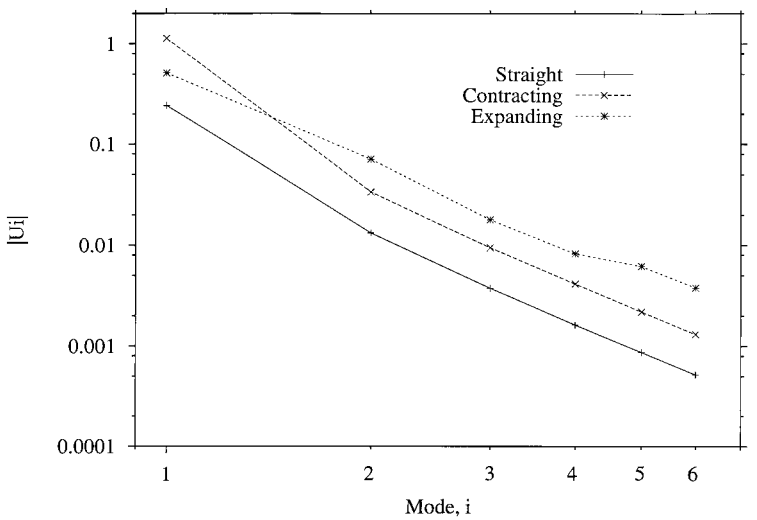

Figure 13. Rate of mode convergence for flow inside straight, contracting, and expanding cavities. The magnitude of the velocity coefficients is plotted against mode i for each case.

veloping free surface flow between two co-axial cylinders of arbitrary shape are obtained in the narrow-gap limit. The flow field is expanded over the gap using the parabolic profile for the leading mode and odd Chandrasekhar functions for the remaining modes. This constitutes a complete set of orthonormal functions for the flow representation. The equations that govern the expansion coefficients are then derived by using the Galerkin projection method. The problem is further reduced by using the conservation of mass to express the expansion coefficients at any axial location in terms of those at the front location. Finally, the momentum equation is integrated between the annular channel exit ($x=0$) to the front location ($x=L$), yielding a coupled differential–algebraic system in the velocity coefficients, the flow rate, the front location, and the pressure at $x=0$. It is shown, under different conditions of flow, cavity geometry and aspect ratio, that only two to three modes are needed for reasonable convergence to be attained. Figure 13 summarizes the level of errors involved for each geometry considered. The figure also reflects the fast rate of mode convergence for flow inside straight, contracting, and expanding cavities. The magnitude of the velocity coefficients is plotted against mode i for each case, which shows (roughly) that $|U_i| = 0.1i^{-3}$ for straight, $0.3i^{-3}$ for contracting, and $0.1i^{-0.6}$ for expanding cavities.

Although some of the geometrical complexities are emphasized in this study, such as the flow inside expanding and contracting cavities, other more realistic configurations could also be considered using the same methodology. Obviously, the current study is relevant to die flow, injection molding, and die casting [25, 26]. These processes involve usually non-isothermal effect and solidification that are not accounted for in the present work. Other effects such as non-Newtonian effects and turbulence are also not addressed. It is, however, important to observe that the proposed formulation is inherently nonlinear, unlike existing approaches in thin film flow, and is therefore amenable to treat additional geometrical and material nonlinearities. Some of these aspects have already been recently addressed by Khayat and coworkers [27–31].

ACKNOWLEDGEMENTS

This work is supported by the Natural Sciences and Engineering Council of Canada.

REFERENCES

1. Hele-Shaw HS. The flow of water. *Nature* 1898; **58**:34.
2. Richardson S. Hele-Shaw flows with a free boundary produced by the injection of fluid into a narrow channel. *Journal of Fluid Mechanics* 1972; **56**:609.
3. Hieber CA, Shen SF. A finite-element/finite-difference simulation of the injection molding filling process. *Journal of Non-Newtonian Fluid Mechanics* 1980; **70**:1.
4. Zienkiewicz OC, Heinrich JC. A unified treatment of steady-state shallow water and two-dimensional Navier–Stokes equations—Finite element penalty function approach. *Computer Methods in Applied Mechanics Engineering* 1979; **17/18**:673.
5. Friedrichs B, Gueceri SI. A novel hybrid numerical technique to model 3-D fountain flow in injection molding processes. *Journal of Non-Newtonian Fluid Mechanics* 1993; **49**:141.
6. Chang RT, Powell TM, Dillon TM. Numerical models of wind driven circulation in lakes. *Applied Mathematical Modeling* 1976; **1**:141.
7. Weare RJ. Finite element or finite difference methods for the two-dimensional shallow water equations. *Computer Methods in Applied Mechanics Engineering* 1976; **7**:351.
8. Floryan JM, Rasmussen H. Numerical methods for viscous flows with moving boundaries. *Applied Mechanical Review* 1989; **42**:323.
9. Nickell RE, Tanner RI, Caswell B. The solution of viscous incompressible jet and free-surface flows using finite element method. *Journal of Fluid Mechanics* 1974; **65**:189.
10. Siliman WJ, Scriven LE. Separating flow near a static contact line: slip at a wall and shape of a free surface. *Journal of Computational Physics* 1980; **34**:287.
11. Ruschak KJ. A method of incorporating free boundaries with surface tension in finite element fluid flow simulation. *International Journal for Numerical Methods in Engineering* 1980; **15**:639.
12. Kawahara M, Miwa T. Finite element analysis of wave motion. *International Journal for Numerical Methods in Engineering* 1984; **20**:1193.
13. Bach P, Hassager O, An algorithm for the use of the Lagrangian specification in Newtonian fluid mechanics and applications to free surface flows. *Journal of Fluid Mechanics* 1985; **152**:173.
14. Ramaswany B, Kawahara M. Lagrangian finite element analysis applied to viscous free surface fluid flow. *International Journal for Numerical Methods in Fluids* 1987; **7**:953.
15. Chipada S, Jue TC, Joo SW, Wheeler MF, Ramaswamy R. Numerical simulation of free-boundary problems. *Computational Fluid Dynamics* 1996; **7**:91.
16. Khayat RE, Derdouri A, Hebert LP. A boundary-element approach to three-dimensional gas-assisted injection molding. *Journal of Non-Newtonian Fluid Mechanics* 1995; **57**:253.
17. Khayat RE, Raducanu P. A coupled finite element/boundary element approach for the three-dimensional simulation of air venting in blow molding and thermoforming. *International Journal for Numerical Methods in Engineering* 1998; **43**:151.
18. Khayat RE, Marek K. An adaptive boundary-element lagrangian approach to 3D transient free-surface flow of viscous fluids. *Engineering and Analytical Boundary Elements* 1999; **23**:111.
19. Wrobel LC. The dual reciprocity boundary element formulation for nonlinear problems. *Computer Methods in Applied Mechanics Engineering* 1987; **65**:147.
20. Nowak AJ. Application of the multiple reciprocity method for solving nonlinear problems. In *Advanced Computational Methods in Heat Transfer II*, *Vol I*: *Conduction*, *Radiation and Phase Change*. Wrobel LC, Brebbia CA, Nowak AJ (eds). Computational Mechanics Publications, 1995.
21. Neves AC, Brebbia CA. The multiple reciprocity boundary element method for transforming domain integrals to the boundary. *International Journal for Numerical Methods in Engineering* 1991; **31**:709.
22. Frayce D, Khayat RE. A dual reciprocity boundary element approach to three-dimensional transient heat conduction as applied to materials processing. *Numerical Heat Transfer A* 1996; **29**:243.
23. Hamrock BJ. *Fundamentals of Fluid Film Lubrication*. McGraw-Hill, 1994.
24. Chandrasekhar S. *Hydrodynamic and Hydromagnetic Stability*. Dover: New York, 1961.
25. Agassant JF, Avenas P, Sergent JPh, Carreau PJ. *Polymer Processing*: *Principles and Modeling*. Hanser Publishers, 1991.
26. Middleman S. *Fundamentals of Polymer Processing*. McGraw-Hill, 1977.
27. Khayat RE, Welke S. Influence of inertia, gravity and substrate topography on the transient coating flow of a thin fluid film. *Physics of Fluids* 2001; **13**:355.
28. Zhang J, Khayat RE. A Lagrangian boundary element approach to transient three-dimensional free surface flow in thin cavities. *International Journal for Numerical Methods in Engineering* (in press).

29. Khayat RE. Transient two-dimensional coating flow of a viscoelastic fluid film on a substrate of arbitrary shape. *Journal of Non-Newtonian Fluid Mechanics* 2001; **95**:199–233.
30. Siddique M, Khayat RE. A low-dimensional approach to linear and non-linear heat conduction in periodic domains. *Numerical Heat Transfer A* 2000; **38**:719–738.
31. Khayat RE. Transient free-surface flow inside thin cavities of viscoelastic fluids. *Journal of Non-Newtonian Fluid Mechanics* 2000; **91**:15.

